Article

An Observational Study of Entrainment Rate in Deep Convection

Xiaohao Guo [1,2], Chunsong Lu [1,2], Tianliang Zhao [1,*], Guang J. Zhang [3] and Yangang Liu [4]

[1] Collaborative Innovation Center on Forecast and Evaluation of Meteorological Disasters, Key Laboratory for Aerosol-Cloud-Precipitation of China Meteorological Administration, Key Laboratory of Meteorological Disaster of Ministry of Education, Nanjing University of Information Science and Technology, Nanjing 210044, China; E-Mails: gxhwqy54@gmail.com (X.G.); luchunsong110@gmail.com (C.L.)

[2] Jiangsu Research Institute of Meteorological Science, Nanjing 210008, China

[3] Scripps Institution of Oceanography, University of California, San Diego, CA 92093, USA; E-Mail: zhangguangjun1960@gmail.com

[4] Biological, Environmental and Climate Science Department, Brookhaven National Laboratory, Upton, NY 11973, USA; E-Mail: lyg@bnl.gov

[*] Author to whom correspondence should be addressed; E-Mail: tlzhao@nuist.edu.cn.

Abstract: This study estimates entrainment rate and investigates its relationships with cloud properties in 156 deep convective clouds based on *in-situ* aircraft observations during the TOGA-COARE (Tropical Ocean Global Atmosphere Coupled Ocean Atmosphere Response Experiment) field campaign over the western Pacific. To the authors' knowledge, this is the first study on the probability density function of entrainment rate, the relationships between entrainment rate and cloud microphysics, and the effects of dry air sources on the calculated entrainment rate in deep convection from an observational perspective. Results show that the probability density function of entrainment rate can be well fitted by lognormal, gamma or Weibull distribution, with coefficients of determination being 0.82, 0.85 and 0.80, respectively. Entrainment tends to reduce temperature, water vapor content and moist static energy in cloud due to evaporative cooling and dilution. Inspection of the relationships between entrainment rate and microphysical properties reveals a negative correlation between volume-mean radius and entrainment rate, suggesting the potential dominance of homogeneous mechanism in the clouds examined. In addition, entrainment rate and environmental water vapor content show similar tendencies of variation with the

distance of the assumed environmental air to the cloud edges. Their variation tendencies are non-monotonic due to the relatively short distance between adjacent clouds.

Keywords: entrainment rate; deep convection; aircraft observations

---

1. Introduction

Convective parameterization significantly influences the cloud-radiation-climate interactions in models [1], as well as the simulations of precipitation [2], typhoon [3] and Madden-Julian Oscillation [4]. As an important parameter in convective parameterization schemes, entrainment rate (λ) affects the vertical transport of heat and moisture in convective clouds [5]. The increase of λ could even delay the diurnal phase of precipitation of convective clouds [6]. Therefore, λ has been studied intensively over the past decades.

Most of the estimations of λ based on observational data have focused on non-precipitating shallow convection. In the early 1970s, Betts [7] inferred the correlation of conserved quantities between cloud and environment and developed a bulk-plume approach that has been widely used since then. For example, using total water content as a conserved quantity, Gerber *et al.* [8] obtained the vertical distribution of λ in maritime shallow convection with an average value of 1.3 km^{-1}. Using the same conserved quantity from shallow convection off the coast of Hawaii, US, Raga *et al.* [9] also obtained the average λ to be 1.3 km^{-1}.

Besides the bulk-plume approach, Jensen and Del Genio [10] estimated λ in convective clouds using the vertical variation of potential temperature in cloud obtained from surface-based remote sensing data. Based on the conservation of cloud mass, total water content and moist static energy, Norgren *et al.* [11] estimated the ratio of entrained mass to the total cloud mass and found that this ratio increased with height.

Unlike shallow convection, the estimation of λ in deep convection has been mostly based on numerical simulations. For instance, applying the bulk-plume approach to large eddy simulations, Del Genio *et al.* [12] found that λ decreased in the development from shallow into deep convection and the surprisingly large value in mid- and upper troposphere was unique to continental convection, *i.e.*, it was larger than the corresponding maritime value. Using a simple entraining plume model commonly used in parameterization of deep convection [13], Khairoutdinov and Randall [14] also found a smaller λ in deep convection compared to that in shallow convection, and found that the least entraining cloud could be modeled rather well by the entraining plume with $\lambda = 0.1$ km^{-1}. Based on large eddy simulations, de Rooy *et al.* [15] calculated λ in maritime deep convection and the result showed that λ decreased from 1.5 km^{-1} to 0.1 km^{-1} with height below 2 km height and was roughly constant (~0.1 km^{-1}) above 2 km height.

The abovementioned studies have improved our understanding of the characteristics of λ. However, observational studies about λ in deep convection are rare, especially for probability density function (PDF) of λ, relating λ to cloud physical parameters, and considering the effects of different sources of entrained air on estimated λ. The objective of this work is to fill this gap by estimating entrainment rate in deep convection using aircraft observations from the TOGA-COARE (Tropical Ocean Global

Atmosphere Coupled Ocean Atmosphere Response Experiment) field campaign, which was conducted over the western Pacific from November 1992 to February 1993.

2. Method and Data

2.1 Method

The estimated approach in Gerber *et al.* [8] is used whereby λ is estimated from the difference of a conserved quantity (ϕ) between cloud and environment:

$$\lambda = \frac{\partial \phi_c}{\partial z} \frac{1}{\phi_e - \phi_c},$$

(1)

where z is height, ϕ_c and ϕ_e denote conserved quantities in the cloud and environment, respectively.

Moist static energy (MSE) is a particularly useful quantity because it provides a useful way of linking cloud thermodynamics and dynamics to study cloud mixing and entrainment processes [14]. Here, MSE is used as the conserved quantity because of its conservation in both dry and wet adiabatic processes and in the processes of entrainment and mixing in precipitating clouds:

$$MSE = c_p T + gz + L_v q,$$

(2)

where c_p is specific heat at constant pressure, T is temperature, g is acceleration of gravity, L_v is latent heat of condensation and q is specific humidity, respectively. Some other studies also used MSE as the conserved quantity when estimating λ using the tracer budget approach [16,17].

In Equation (1), $\partial \phi_c/\partial z$ is the vertical gradient of ϕ_c in cloud. Here, $\partial \phi_c/\partial z$ is calculated as the difference between the MSE at the aircraft observation level and the cloud base divided by the depth between the two levels; ϕ_c is calculated as the mean MSE of the two levels, assuming that λ is evenly distributed, *i.e.*, constant from the cloud base to the observation level. When we assume the entrained air to be the same as the average environmental air far away from the clouds, ϕ_e is taken as the MSE at the level half way between the observation level and the cloud base from the vertical profile of environmental MSE. The method to obtain this profile will be introduced in the next section. On the other hand, when we assume the entrained air to come from the vicinity of the cloud edge as in some recent studies [18–20] in Section 3.3, ϕ_e is calculated as the mean value between the environmental MSE near the cloud edge at the observation level and MSE at the cloud base. Horizontal distances (D) between this nearby environmental MSE and the cloud edges are 100, 200, 300, …, and 800 m, with an interval of 100 m. The dependence of λ on D is examined in Section 3.3.

2.2. Data

TOGA-COARE was a large international field experiment conducted in 1992–1993 to study the atmospheric and oceanic processes over the "warm pool" region of the western Pacific [21]. There were 32 aircraft observation missions (R1~R32) of deep convection carried out by the NCAR (National Center for Atmospheric Research) Electra research aircraft and the total flight time was 204 hours. The horizontal flights were approximately at the heights of 1500 m, 3000 m and 5000 m and all the data from these heights are used in this study. The primary observation instruments and observed properties include FSSP-100 probe (cloud droplet size distribution, range from 2 to 45 μm in diameter;

accuracy: ±20% in diameter and ±16% in concentration), radome gust probe (updraft velocity), Ophir Ⅲ radiometer (temperature), T-Electric hygrometer (dew-point temperature and water vapor mixing ratio, accuracy: ±5 °C), and 260X OAP cloud probe (range from 40 to 600 μm in diameter).

Individual clouds need to be identified before applying the abovementioned approach to the TOGA-COARE flight observational data. The following criteria are used in this study. Liquid water content (LWC) must be larger than 0.001 g·m^{-3} and cloud droplet number concentration (N) must be greater than 10 cm^{-3} [22]. Given that the bulk-plume approach is only appropriate for developing clouds, the percentage of updraft within a cloud must exceed 80% [8] and the cloud penetration time must be longer than 5 s [11] to eliminate the clouds that are too small. There are a total of 156 clouds satisfying these criteria. One hundred and twenty-eight clouds have temperature higher than 0 °C. The temperature in the remaining 28 clouds is in the range of −10–0 °C and supercooled liquid water is expected to be dominant with negligible ice particles [23]. The PDF of horizontal cloud size (calculated as the product of the penetration time in cloud and the aircraft speed) is close to lognormal distribution and roughly decreases with the increasing horizontal size when size is larger than 600 m (Figure 1). This result is similar to previous observations [24] and simulations [25], and will be utilized to examine the correlation between λ and cloud size in Section 3.
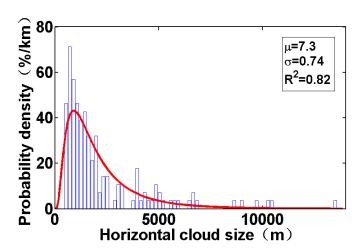

Figure 1. Probability density function of horizontal cloud size. The red line is fitted lognormal distribution. Mean (μ), standard deviation (σ) of the logarithm of horizontal cloud size and coefficients of determination (R^2, a statistical measure of how well the regression line approximates the real data points) for the lognormal fit are also provided.

The specific procedures for estimating the cloud base are as follows: Calculate the temperature (T) and dew-point temperature (T_d) obtained from the aircraft vertical sounding in the environment far away from the cloud, apply a moving average with 200 m in the vertical to filter out small-scale noises, and then obtain the vertical profile of MSE. Lifting condensation level (LCL, the black horizontal line and approximately 400m high in Figure 2), which is assumed to be the cloud base, is obtained from the T and T_d at the height of approximately 100 m where MSE is the largest (Figure 2). As an example, Figure 2 shows both the original and averaged vertical profiles of T and T_d and the corresponding MSE profile in the R28 case (6 February 1993); the red points represent the mean MSE values in each cloud.
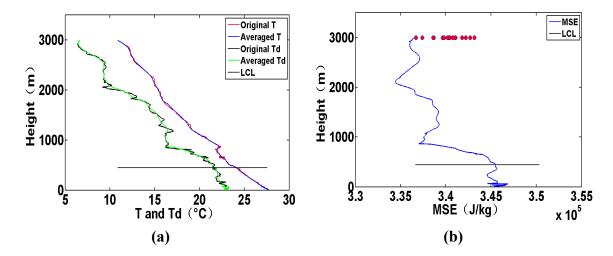
Figure 2. Aircraft vertical sounding of R28 case: (**a**) Temperature (*T*) and dew-point temperature (*T*d) and (**b**) moist static energy (MSE), and the black horizontal lines represent the heights of LCL; the red points in (**b**) represent the mean MSE values in each cloud.
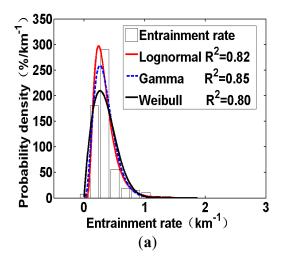
3. Results

3.1. PDF of λ

PDF of λ is important for parameterization because the entrainment process can be treated as a stochastic process and that a more realistic parameterization of convection requires PDF of λ [17,26]. Multiple mass-flux parameterizations [27] and multiple-parcel models [28] also emphasized the importance of representing the PDF of λ.

Table 1. Three fitted probability density functions (PDFs) for entrainment rate (λ) and related parameters.

Function	Form	Meaning of Parameters
Lognormal	$f(\lambda) = \dfrac{1}{\lambda\sigma\sqrt{2\pi}} e^{-\frac{(\ln\lambda - \mu)^2}{2\sigma^2}}$	μ and σ are mean value and standard deviation of $\ln(\lambda)$, respectively.
Gamma	$f(\lambda) = \dfrac{1}{b^a\Gamma(a)} \lambda^{a-1} e^{-\frac{\lambda}{b}}$	a and b are shape and scale parameters, respectively.
Weibull	$f(\lambda) = \dfrac{q}{c}(\dfrac{\lambda}{c})^{q-1} e^{-(\lambda/c)^q}$	c and q are scale and shape parameters, respectively.

In this section, the PDF of λ is investigated with three commonly used PDF-functions, *i.e.*, lognormal, gamma and Weibull distributions. These three PDF distributions and their associated parameters are listed in Table 1. Figure 3 shows the PDF of λ and the corresponding fitted lognormal, gamma and Weibull distributions and their corresponding parameters. The properties of the entrained air in Figure 3 are obtained from the aircraft vertical sounding. The results show that the PDF of λ can be well fitted by the any of these three distributions, with the coefficients of determination larger than 0.80. This is true either for all the 156 clouds (Figure 3a) or only for the 92 clouds collected around 3000 m height (Figure 3b). In terms of the coefficient of determination, gamma (0.85 and 0.87 in

Figures 3a and 3b, respectively) is slightly better than the other two distributions (0.82, 0.84 and 0.80, 0.86 in Figures 3a and 3b, respectively).
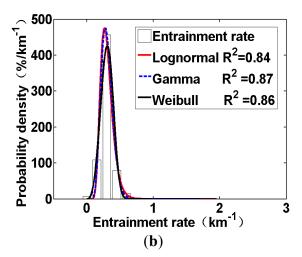

Figure 3. Probability density functions (PDFs) of entrainment rate with the properties of entrained air from the aircraft vertical sounding for (**a**) all 156 clouds, and (**b**) 92 clouds the observational heights of which are around 3000m. The coefficients of determination (R^2) for the lognormal, gamma and Weibull fits are also given.

Lu *et al.* [20] found that the PDF of λ was well fitted by lognormal distribution in shallow convection assuming that the entrained air was from the aircraft vertical sounding; their mean and standard deviation of the lognormal distribution were −0.41 and 0.65, respectively. The corresponding mean value and standard deviation of lognormal distribution in Figure 3a are −1.19 and 0.49, respectively (Table 2). Comparatively, the mean value in deep convection is smaller than in shallow convection, which is consistent with some numerical studies [12,14,29,30]. In addition, Cheng *et al.* [31] studied the PDF of λ in shallow convection on the scale of 5 m and they found that Weibull distribution was better than lognormal and gamma distribution to describe the PDF of λ. However, when they used the cloud-mean λ to fit PDF, they found lognormal was the better one. The results suggest that the optimal distribution of λ is different in shallow and deep convection, and may also be related to the scale of interest. To the authors' knowledge, this study is the first one on the PDF of λ in deep convection from the observational perspective.

Table 2. Related parameters for the three fitted probability density functions (PDFs) of entrainment rate (λ) in Figure 3.

	μ	σ	a	b	c	q
156 clouds	−1.19	0.49	4.04	0.09	0.39	1.88
92 clouds	−1.24	0.31	12.02	0.03	0.33	3.69

3.2. Relationships between λ and Cloud Properties

The PDF of λ indicates that different clouds have different values of λ; thus it is interesting to examine how cloud properties correspond to different λ [28]. The relationships of cloud properties to λ are important to understanding the interactions of dynamics, thermodynamics and microphysics in clouds at the 3000 m level (the aircraft observation level).

Microphysical properties change at different heights above the cloud base. To focus on the effects of λ on cloud microphysics and other related properties, only the data at the observational height around 3000 m are analyzed (Figure 4a–e). The reason to choose this height is that the number of sampled clouds is the largest; there are 92 out of the total 156 clouds at this height. It is noteworthy that the corresponding scatter plots at other heights (not shown) have similar tendencies.
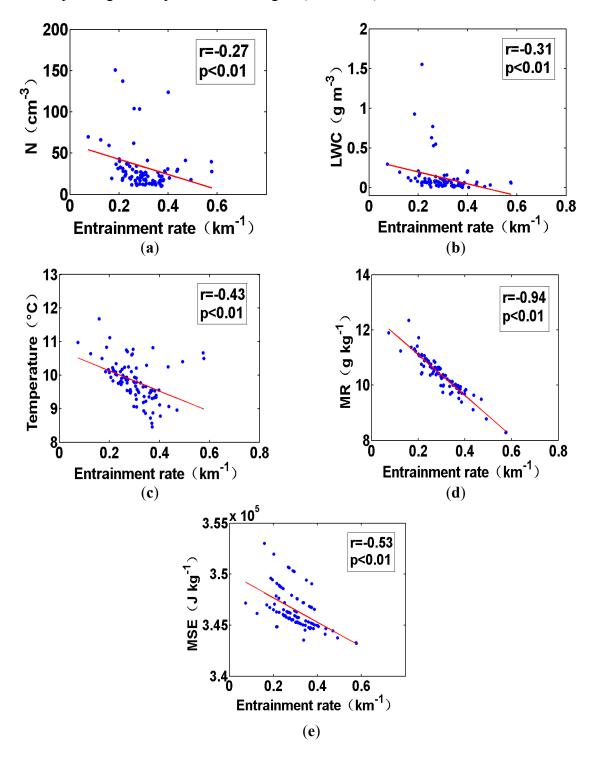

Figure 4. Scatter plots of entrainment rate *vs.* (**a**) cloud droplet number concentration (*N*), (**b**) liquid water content (LWC), (**c**) temperature (*T*), (**d**) water vapor mixing ratio (MR), and (**e**) moist static energy (MSE) in clouds. Each legend provides the correlation coefficient (*r*) and the *p* value (a function used for testing a statistical hypothesis) of the correlation.

Figure 4 shows the relationships of λ to some key cloud properties. The correlation coefficients (r) in these figures, especially in Figure 4a,b, are relatively low, according to the criterion of Asuero *et al.* [32]. The reason is that these correlations are affected by many factors that are not included in the analyses. For example, Figure 4a shows the correlation between number concentration and entrainment rate. Besides entrainment rate, number concentration is affected by other factors, e.g., aerosol number concentration, aerosol chemical composition and vertical velocity. Thus, the correlation coefficient between number concentration and entrainment rate is expected to be low. Although the $|r|$ is low, all correlations satisfy $p < 0.01$; thus, the results are still reliable. In addition, the weak negative correlations between entrainment rate and cloud microphysics are still similar to those found for shallow convection in other studies in spite of the noisy data [22,31]; the mechanism is that a larger entrainment rate results in more dilution and evaporation of cloud droplets.
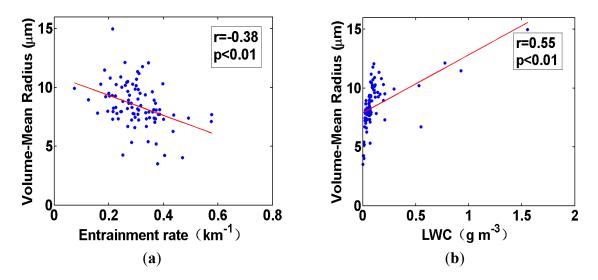

Figure 5. Scatter plots of (**a**) volume-mean radius of cloud droplets *vs.* entrainment rate and (**b**) volume-mean radius *vs.* liquid water content. Each legend provides the correlation coefficient (*r*) and the *p* value of the correlation.

Figure 5 further shows the correlation between volume-mean droplet radius (R_v) and λ, which provides important information on entrainment-mixing mechanisms [33,34]. In the case of homogeneous mechanism, all droplets within a cloud evaporate and their droplet sizes almost decrease at the same time, so the relationship between λ and cloud droplet radius should also be negatively correlated. In the case of extreme inhomogeneous entrainment-mixing mechanism, some cloud droplets that are close to dry air would evaporate completely while the remaining droplets do not evaporate; therefore, the mean droplet radius does not show significant variation with the increasing λ. Some studies proposed that the actual scenario in atmospheric clouds is between the two extreme mechanisms [33,35,36]. The negative correlation between λ and R_v indicates that the entrainment-mixing mechanism possibly tends to homogeneous. Figure 5b reveals that the relationship between R_v and LWC is significantly positive and also indicates the potential dominance of homogeneous entrainment-mixing mechanism This is similar to the mechanism in the lower part of stratocumulus cloud in Lu *et al.* [33] and cumulus cloud in Burnet and Brenguier [37]. Some other observational studies also found that homogeneous mechanism dominated in their analyzed clouds [22,36,38]. It is noteworthy that the entrainment of Cloud Condensation Nuclei (CCN) from

environmental air and the activation of CCN can cause some uncertainties in the analyses on entrainment-mixing mechanisms, because the activation of entrained CCN can increase the number concentration of small cloud droplets. Since aircraft observation cannot distinguish the source of small droplets, whether from evaporation of big droplets or activation of entrained CCN, high-resolution models could be good tools to examine the effect of secondary activation on entrainment-mixing mechanisms, which deserves further study.

The cloud properties in Figures 4 and 5 could be affected by precipitation. The relationship between precipitation and entrainment rate is added as Figure 6. Liquid water content from the 260X probe is taken to be precipitation. Figure 6 shows that only when λ is smaller than ~0.4 km^{-1}, precipitation begins to appear. Entrained environmental air promotes the dilution and evaporation in cloud and hinders the growth of large cloud droplets (Figure 5) and the collision coalescence and further restrains precipitation. Qualitatively, more intensive precipitation corresponds to larger entrainment rate, which further causes smaller N, LWC, T, MR, MSE and Rv. Precipitation is produced from cloud development. However, after precipitation appears, precipitation begins to weaken cloud development. Cloud models or cloud-resolving models could be good tools used to study the quantitative effect of precipitation in the future.
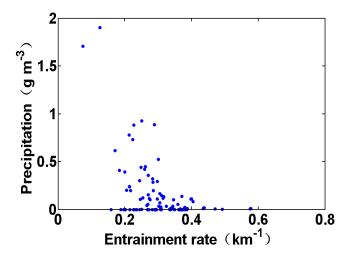

Figure 6. Scatter plots of entrainment rate *vs.* precipitation.

Macrophysical cloud properties could influence λ as well. Figure 7 shows the influence of the horizontal cloud size on obtained λ. The correlation here is still low and the similar reason has been discussed in the analysis on Figure 4. The positive correlation between λ and the reciprocal of cloud size is similar to theoretical expectation that for smaller clouds, turbulence and entrainment near cloud edge could more significantly influence cloud properties. Generally speaking, for large clouds, the environmental dry air is relatively far away from the cloud cores. Therefore, dilution from the environmental entrainment does not affect the clouds as much. The inverse correlation between λ and cloud size has been used by some parameterizations [13,39–41], and our observations support such use to some extent. The reason for using the reciprocal of cloud size is to make the relationship linear.
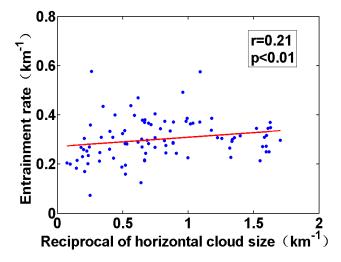
Figure 7. Entrainment rate as a function of the reciprocal of horizontal cloud size and also provided in legend is the correlation coefficient (*r*) and the *p* value of the correlation.

3.3. Effects of Different Sources of Environmental Air on λ

Environmental air usually entrains into cloud across the interface between clouded air and clean air, such as lateral interface which is assumed in this study. The properties of dry air are often assumed to be obtained from the aircraft vertical sounding far away from cloud edges when using the tracer budget approach [8]. However, some studies pointed out that the entrained air derives from the humid shell around the cloud [18,19]. In addition, the optimal selection of *D* (defined in Section 2.1) in different models is also inconsistent [18]. Therefore, the effects of different assumed sources of environmental air on estimated λ for deep convection needs to be further investigated. The purpose of setting *D* to different values in this study is to test the sensitivity of the estimated λ to the varying *D* values.

Horizontal distances (*D*) between entrained air and cloud edges are assumed as 100, 200, 300 …, and 800 m in Figure 8. Figure 8a illustrates the effects of different sources on λ, where the average λ (including the total 156 clouds) roughly decreases with increasing *D* except a weak increase of λ when *D* is from 400 to 600 m. The PDF in Figure 9 shows that many distances between adjacent clouds are within 1 km. This indicates that the non-monotonic variation in Figure 8a may be related to the relatively short distances between adjacent clouds and their mutual influences. In order to gradually eliminate this influence from other clouds, such as excluding the clouds with distances less than 300, 600 and 900 m (Figure 8b–d) from the total 156 clouds, the increasing tendencies of λ around 400 m gradually disappear.

The similar trend also appears in the variation of the environmental MR with *D*. MR generally decreases with increasing *D*, but increases when *D* is from 400 to 500 m (Figure 8a); this increasing trend gradually disappears in Figure 8b–d when excluding clouds that are close to their neighboring clouds. Figure 8d shows that both λ and MR monotonically decrease with increasing *D*, which is similar to the results in Lu *et al.* [20]. It is noteworthy that they eliminated the clouds that are too close to their surrounding clouds using a time threshold.
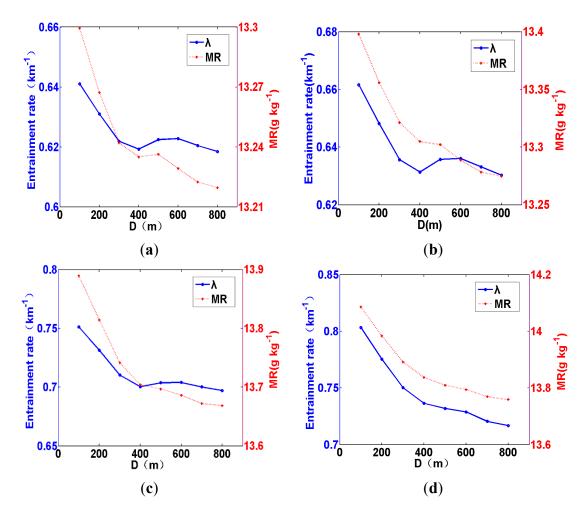
Figure 8. Entrainment rate and environmental water vapor mixing ratio as a function of distance of the assumed entrained dry air to the cloud edges when (**a**) including all clouds, and excluding the clouds the distance between which and their nearby clouds are less than (**b**) 300 m, (**c**) 600 m, and (**d**) 900 m.

The above analysis suggests that a different assumed source of environmental air has significant effects on the MR in entrained air and the computed λ. In fact, the relationship between MR and λ results essentially from Equations (1) and (2). The average λ obtained from the aircraft vertical sounding is 0.4 km^{-1}, which is smaller than the results assuming that the dry air is obtained from the nearby environmental air; the reason is that the environmental MR (11.5 g·kg^{-1}) from the vertical sounding is smaller. Similar results have also been found by some numerical [18,19] and observational studies [20]. In addition, Romps [18] suggested that the entrained air of a convective cloud derives from the humid shell itself or other clouds by large-eddy simulation. Our study confirms his simulated results from an observational perspective. Therefore, apart from the selection of the optimal D to estimate λ as proposed by Lu *et al.* [20], the influence from surrounding clouds to the estimation of λ also needs to be considered for the parameterization of λ in models.
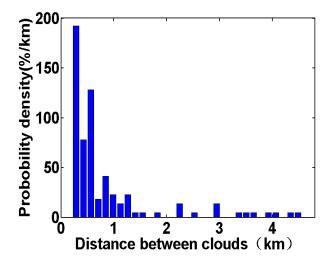
Figure 9. The probability density function of the distance between adjacent clouds.

4. Conclusions

Entrainment rates (λ) in the 156 growing deep convective clouds from the TOGA-COARE field campaign are estimated using the bulk-plume approach. Probability density function (PDF) of λ, the relationships between λ and cloud properties, and the effects of dry air sources on the calculated λ in deep convection are examined. To the authors' knowledge, this is the first study of such kind in deep convection from an observational perspective.

It is found that PDF of λ can be well fitted by lognormal, gamma or Weibull distribution. More entrained environmental dry air possibly leads to decreases in cloud-mean number concentration (N) and liquid water content (LWC) due to dilution and evaporation of cloud droplets in spite of low correlation for noisy data. Because of evaporative cooling and dilution, entrainment also reduces temperature (T) and water vapor mixing ratio (MR) in clouds. With the simultaneous decreases in T and MR, a large λ corresponds to a decrease in the cloud-mean moist static energy (MSE). The negative correlation between volume-mean radius (Rv) and λ possibly indicates the potential dominance of the homogeneous entrainment-mixing mechanism. The entrainment of CCN and its activation is another factor that leads to the increase of small cloud droplets and needs to be further investigated. In addition, more intensive precipitation corresponds to larger λ, which further causes smaller N, LWC, T, MR, MSE and Rv.

Different assumed sources of environmental air have significant effects on the MR in entrained air and the estimated λ. Entrainment rate and environmental MR show similar variation tendencies with the increasing distance (D) of the assumed environmental air to the cloud edges. The average λ obtained from aircraft vertical sounding is smaller than the λ assuming environmental air is near the cloud because of comparatively smaller MR vertical sounding. The relatively short distances between adjacent clouds cause the variation tendencies of both λ and water vapor content to be non-monotonic. Both the selection of the optimal D and the influence from surrounding clouds need to be fully considered for the parameterization of λ in models.

Acknowledgments

Author Contributions

Xiao Guo prepared the original manuscript. Chunsong Lu, Tianliang Zhao, Guangjun Zhang and Yangang Liu made a lot of modifications.

Conflicts of Interest

The authors declare no conflict of interest

References

1. Tost, H.; Jockel, P.; Lelieveld, J. Influence of different convection parameterisations in a GCM. *Atmso. Chem. Phys.* **2006**, *6*, 5475–5493.
2. Liang, X.Z.; Li, L.; Dai, A.G.; Kunkel, K.E. Regional climate model simulation of summer precipitation diurnal cycle over the United States. *Geophys. Res. Lett.* **2004**, *31*, L24208.
3. Li, X. Sensitivity of WRF simulated typhoon track and intensity over the Northwest Pacific Ocean to cumulus schemes. *Sci. China Earth Sci.* **2013**, *56*, 270–281.
4. Zhang, G.J.; Song, X. Interaction of deep and shallow convection is key to Madden-Julian Oscillation simulation. *Geophys. Res. Lett.* **2009**, 36, L09708.
5. Siebesma, A.P.; Cuijpers, J.W.M. Evaluation of parametric assumptions for shallow cumulus convection. *J. Atmos. Sci.* **1995**, *52*, 650–666.
6. Wang, Y.; Li, Z.; Kevin, H. Effect of convective entrainment/detrainment on the simulation of the topical precipitation diurnal cycle. *Mon. Weather Rev.* **2007**, *135*, 567–585.
7. Betts, A.K. Parametric interpretation of trade-wind cumulus budget studies. *J. Atmos. Sci.* **1975**, *32*, 1934–1945.
8. Gerber, H.E.; Frick, G.M.; Jensen, J.B.; Hudson, J.G. Entrainment, mixing, and microphysics in trade-wind cumulus. *J. Meterol. Soc. Jpn.* **2008**, *86*, 87–106.
9. Raga, G.B.; Jensen, J.B.; Baker, M.B. Characteristics of cumulus band clouds off the coast of Hawaii. *J. Atmos. Sci.* **1990**, *47*, 338–356.

10. Jensen, M.P.; Genio, A.D.D. Factors limiting convective cloud-top height at the ARM Nauru Island climate research Facility. *J. Climate* **2006**, *19*, 2015–2117.

11. Norgren, M.S.; Small, J.D.; Jonsson, H.H.; Chuang, P.Y. Observational estimates of detrainment and entrainment in non-precipitating shallow cumulus. *Atmos. Chem. Phys. Discuss.* **2014**, *14*, 21785–21827.

12. Genio, D.; Anthony, D.; Wu, J.B. The role of entrainment in the diurnal cycle of continental convection. *J. Climate* **2010**, *10*, 2722–2738.

13. Arakawa, A.; Schubert, W.H. Interaction of a cumulus cloud ensemble with the large-scale environment, Part I. *J. Atmos. Sci.* **1974**, *31*, 674–701.

14. Khairoutdinov, M.; Randall, D. High-resolution simulation of shallow to deep convection transition over land. *J. Atmos. Sci.* **2006**, *63*, 3421–3436.

15. de Rooy, W.C.; Bechtold, P.; Fröhlich, K.; Hohenegger, C.; Jonker, H.; Mironov, D.; Siebesma, A.P.; Teixeira, J.; Yano, J.-I. Entrainment and detrainment in cumulus convection: An overview. *Q. J. R. Meteorol. Soc.* **2011**, *00*, 2–29.

16. Martin, S.S.; Paul, A.O. Influence of entrainment on the thermal stratification in simulations of radiative-convective equilibrium. *Geophys. Res. Lett.* **2013**, *40*, 5223–5227.

17. Böing, S.J.; Jonker, H.J.J.; Nawara, W.A.; Siebesma, A.P. On the deceiving aspects of mixing diagrams of deep cumulus convection. *J. Atmos. Sci.* **2014**, *71*, 56–68.

18. Romps, D.M. A direct measure of entrainment. *J. Atmos. Sci.* **2010**, *67*, 1908–1927.

19. Dawe, J.T.; Austin, P.H. The influence of the cloud shell on tracer budget measurements of LES cloud entrainment. *J. Atmos. Sci.* **2011**, *68*, 2909–2920.

20. Lu, C.S.; Liu, Y.G.; Niu, S.J.; Vogelmann, A.M. Lateral entrainment rate in shallow cumuli: Dependence on dry air sources and probability density functions. *Geophys. Res. Lett.* **2012**, *39*, L20812.

21. Webster, P.J.; Lucas, R. TOGA COARE: The coupled ocean–atmosphere response experiment. *Bull. Amer. Meteor. Soc.* **1992**, *73*, 1377–1416.

22. Lu, C.S.; Liu, Y.G.; Niu, S.J.; Vogelmann, A.M. Empirical relationship between entrainment rate and microphysics in cumulus clouds. *Geophys. Res. Lett.* **2013**, *40*, 2333–2338.

23. Yang, J.; Chen, B.J.; Yin, Y. *Physics of Clouds and Precipitation*; China Meteorological Press: Beijing, China, 2011.

24. Wang, Y.G.; Geerts, B.; French, J. Dynamics of the cumulus cloud margin: An observational study. *J. Atmos. Sci.* **2009**, *66*, 3660–3677.

25. Dawe, J.T.; Austin, P.H. Direct entrainment and detrainment rate distributions of individual shallow cumulus clouds in an LES. *Atmos. Chem. Phys.* **2013**, *13*, 7795–7811.

26. Romps, D.M.; Kuang, Z. Nature *versus* nurture in shallow convection. *J. Atmos. Sci.* **2010**, *67*, 1655–1666.

27. Sušelj, K.; Hogan, T.F.; Teixeira, J. Implementation of a stochastic eddy-diffusivity/mass-flux parameterization into the Navy Global Environmental Model. *Weather Forecast.* **2014**, *29*, 1374–1390.

28. Neggers, R.A.J.; Siebesma, A.P.; Jonker, H.J.J. A multiparcel model for shallow cumulus convection. *J. Atmos. Sci.* **2002**, *59*, 1655–1668.

29. Bretherton, C.S.; Blossey, P.N.; Khairoutdinov, M. An energy-balance analysis of deep convective self-aggregation above uniform SST. *J. Atmos. Sci.* **2005**, *62*, 4273–4292.

30. Kuang, Z.; Bretherton, C.S. A mass-flux scheme view of a high-resolution simulation of a transition from shallow to deep cumulus convection. *J. Atmos. Sci.* **2006**, *63*, 1895–1909.

31. Cheng, M.N.; Lu, C.S.; Liu, Y.G. Variation in entrainment rate and relationship with cloud microphysical properties on the scale of 5 m. *Sci. Bull.* **2015**, *60*, 707–717.

32. Asuero, A.G.; Sayago, A.; Gonzalez, A.G. The correlation coefficient: An overview. *Crit. Rev. Anal. Chem.* **2006**, *36*, 41–59.

33. Lu, C.S.; Liu, Y.G.; Niu, S.J. Examination of turbulent entrainment-mixing mechanisms using a combined approach. *J. Geophys. Res.* **2011**, *116*, D20207.

34. Lu, C.S.; Liu, Y.G.; Niu, S.J.; Endo, S. Scale dependence of enrainment-mixing mechanisms in cumulus clouds. *J. Geophys. Res.* **2014**, *119*, D022265.

35. Andrejczuk, M.; Grabowski, W.W.; Malinowski, S.P.; Smolarkiewicz, P.K. Numerical simulation of cloud-clear air interfacial mixing: Homogeneous *versus* inhomogeneous mixing. *J. Atmos. Sci.* **2009**, *66*, 2493–2500.

36. Lehmann, K.; Siebert, H.; Shaw, R.A. Homogeneous and inhomogeneous mixing in cumulus clouds: Dependence on local turbulence structure. *J. Atmos. Sci.* **2009**, *66*, 3641–3659.

37. Burnet, F.; Brenguier, J.L. Observational study of the entrainment-mixing process in warm convective clouds. *J. Atmos. Sci.* **2007**, *64*, 1995–2011.

38. Jensen, J.B.; Austin, P.H.; Baker, M.B.; Blyth, A.M. Turbulent mixing, spectral evolution and dynamics in a warm cumulus cloud. *J. Atmos. Sci.* **1985**, *42*, 173–192.

39. Tiedtke, M. A comprehensive mass flux scheme for cumulus parameterization in large-scale models. *Mon. Weather Rev.* **1989**, *117*, 1779–1800.

40. Kain, J.S.; Fritsch, J.M. A one-dimensional entraining/detraining plume model and its application in convective parameterization. *J. Atmos. Sci.* **1990**, *47*, 2784–2802.

41. Wagner, T.M.; Graf, H.F. An ensemble cumulus convection parameterization with explicit cloud treatment. *J. Atmos. Sci.* **2010**, *67*, 3854–3869.